Estimating the top altitude of optically thick ice clouds from thermal infrared satellite observations using CALIPSO data

Patrick Minnis,[1] Chris R. Yost,[2] Sunny Sun-Mack,[2] and Yan Chen[2]

Received 11 March 2008; revised 16 April 2008; accepted 9 May 2008; published 17 June 2008.

[1] The difference between cloud-top altitude Z_{top} and infrared effective radiating height Z_{eff} for optically thick ice clouds is examined using April 2007 data taken by the Cloud-Aerosol Lidar and Infrared Pathfinder Satellite Observations (CALIPSO) and the Moderate-Resolution Imaging Spectroradiometer (MODIS). For even days, the difference ΔZ between CALIPSO Z_{top} and MODIS Z_{eff} is 1.58 ± 1.26 km. The linear fit between Z_{top} and Z_{eff}, applied to odd-day data, yields a difference of 0.03 ± 1.21 km and can be used to estimate Z_{top} from any infrared-based Z_{eff} for thick ice clouds. Random errors appear to be due primarily to variations in cloud ice-water content (IWC). Radiative transfer calculations show that ΔZ corresponds to an optical depth of ~1, which based on observed ice-particle sizes yields an average cloud-top IWC of ~0.015 gm^{-3}, a value consistent with in situ measurements. The analysis indicates potential for deriving cloud-top IWC using dual-satellite data. **Citation:** Minnis, P., C. R. Yost, S. Sun-Mack, and Y. Chen (2008), Estimating the top altitude of optically thick ice clouds from thermal infrared satellite observations using CALIPSO data, *Geophys. Res. Lett.*, *35*, L12801, doi:10.1029/2008GL033947.

1. Introduction

[2] Infrared (IR) atmospheric window (~11 μm) radiances are routinely used to estimate cloud-top heights from passive satellite sensors [e.g., *Minnis et al.*, 1995; *Rossow and Schiffer*, 1999]. The cloud effective radiating temperature T_{eff} is estimated from the observed 11-μm brightness temperature T_{11} and matched to local temperature soundings to find the cloud-top height. Although it is recognized that T_{eff} corresponds to some level below the tops of optically thin clouds, it is commonly assumed that optically thick clouds have sharp boundaries. The latter are generally treated as blackbodies with T_{11}, after correcting for atmospheric absorption and cloud particle scattering, assumed to be equivalent to the cloud-top temperature. Recently, *Sherwood et al.* [2004] demonstrated, however, that even deep convective clouds do not have such sharply defined boundaries in the IR spectrum. They found that cloud-top heights derived from the eighth Geostationary Operational Environmental Satellite (GOES-8) were 1–2 km below the convective cloud tops detected by lidar data collected over Florida. Those and other results require new approaches to interpret the infrared brightness temperatures of optically thick clouds. Measurements from active sensors combined with passive infrared radiances are needed to address this outstanding problem.

[3] Until recently, active remote sensing of optically thick clouds has been extremely limited. Ground-based radars and lidars profile the atmosphere continuously, but observe at only one location. They are also unlikely to detect optically thick ice cloud tops because lidars can only penetrate to optical depths of less than about 3 into the cloud and cloud radars often have no returns from smaller ice crystals common at the tops of such clouds. Airborne active sensors sample larger areas during field campaigns and can outline the tops of the clouds, but they collect data for only a few days during a given experiment. With the 2006 launch of the Cloud-Aerosol Lidar and Infrared Pathfinder Satellite Observations (CALIPSO) satellite into orbit behind the *Aqua* satellite in the A-Train, coincident and nearly simultaneous global lidar and infrared radiance measurements are now available. This study uses the measurements from CALIPSO and the *Aqua* Moderate-Resolution Imaging Spectroradiometer (MODIS) to develop a new method to estimate the physical top of optically thick ice clouds from passive IR imager data.

2. Data and Methodology

[4] Like *Aqua*, CALIPSO follows a Sun-synchronous orbit with an approximately 1330-LT equatorial crossing time ~90 s behind *Aqua*. Because CALIPSO is offset by 7–18° east of *Aqua*, the *Aqua* sensors typically observe the CALIPSO ground track at viewing zenith angles VZA of 9–19°. The primary CALIPSO instrument is the Cloud Aerosol Lidar with Orthogonal Polarization (CALIOP), which has 532 and 1064-nm channels for profiling clouds and aerosols [*Winker et al.*, 2007]. The CALIOP, with footprints nominally 70-m wide and sampled every 330 m, allows the global characterization of cloud vertical structure at resolutions up to 30 m. The CALIPSO data used here are the April 2007 Version 1.21 1/3 km cloud height products [*Vaughan et al.*, 2004].

[5] Cloud properties derived from 1-km *Aqua* MODIS radiances using the Clouds and the Earth's Radiant Energy System (CERES) project cloud retrieval algorithms [*Minnis et al.*, 2006] were matched with CALIOP data [see *Sun-Mack et al.*, 2007]. The CERES cloud properties were determined from MODIS radiances using updated versions of the daytime Visible Infrared Solar-Infrared Split Window Technique (VISST) and the nighttime Solar-infrared Infrared Split-window Technique (SIST) [*Minnis et al.*, 1995]. The products include cloud temperature, height, thermodynamic phase, optical depth, effective ice crystal diameter D_e, and other cloud properties.

[1]NASA Langley Research Center, Hampton, Virginia, USA.
[2]Science Systems and Applications, Inc., Hampton, Virginia, USA.

0094-8276/08/2008GL033947$05.00

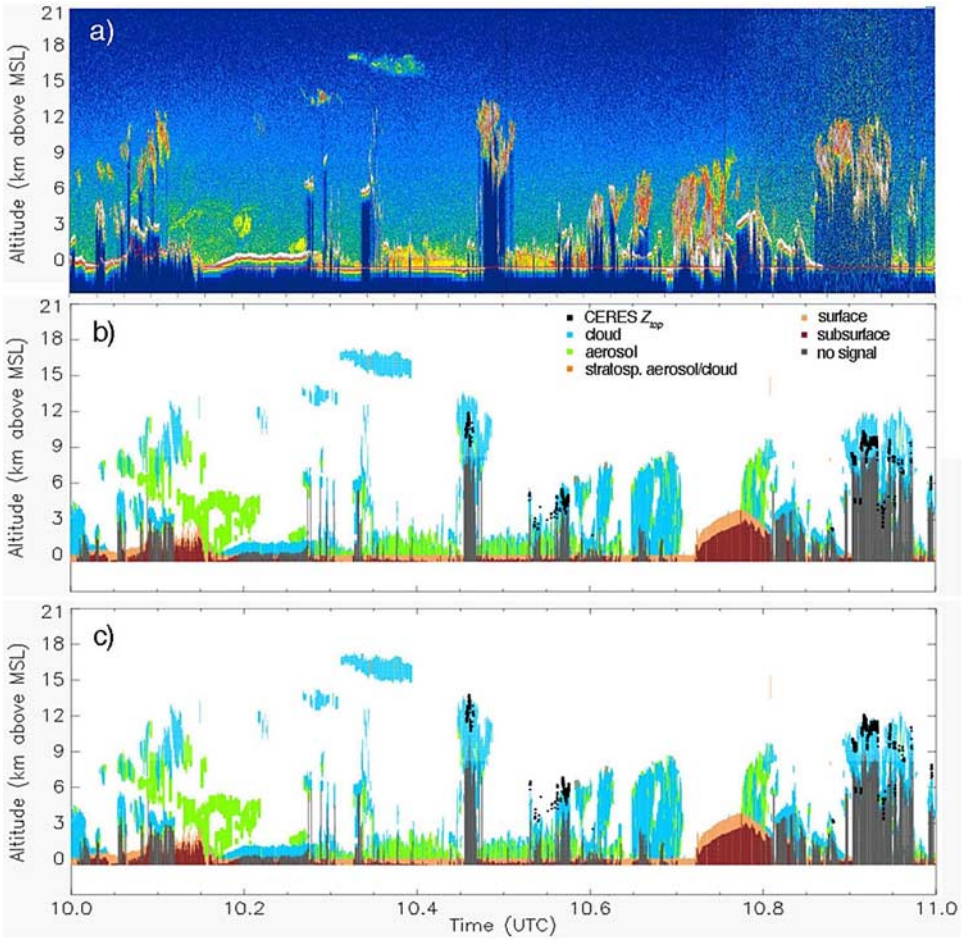

Figure 1. CALIPSO products for 27 April 2007. (a) CALIOP backscatter intensities, (b) CALIPSO feature mask with overlaid CERES-*Aqua*-MODIS cloud-top heights Z_{top} for single-layer optically thick ice clouds, and (c) same as Figure 1b except Z_{top} corrected with equation (1).

[6] The VISST/SIST first determines T_{eff}, which corresponds to the cloud effective height Z_{eff}, located somewhere within the cloud [e.g., *Minnis et al.*, 1990]. Above 500 hPa, Z_{eff} is determined by matching T_{eff} to a local atmospheric temperature sounding. For optically thin ice clouds, an empirical correction is applied to estimate the true cloud-top temperature T_{top} based on cloud emissivity [*Minnis et al.*, 1990]. The true cloud-top altitude Z_{top} for those clouds is the lowest level in the sounding corresponding to T_{top}. Optically thick clouds are assumed to have sharp boundaries and, therefore, most IR radiation reaching the satellite sensor is emitted by the uppermost part of the cloud. In these cases, VISST and SIST assume that T_{eff} is equivalent to T_{top} and $Z_{top} = Z_{eff}$. VISST accounts for the effects of infrared scattering so, for these clouds, T_{eff} is slightly greater than T_{11}.

[7] Matched VISST and CALIPSO data from every even day during April 2007 were selected to develop a relationship between the effective and true cloud-top heights of optically thick ice clouds. Clouds with effective emittance exceeding 0.98 (visible optical depth $\tau > 8$) are considered to be optically thick. This definition includes a wide variety of clouds including thick cirrus and convective cloud anvils and cores. Polar clouds (latitudes >60°) were excluded to avoid mischaracterizing them over ice and snow. The method is tested using the odd-day April 2007 MODIS-CALIPSO non-polar matched data.

3. Cloud-Top Height Correction

[8] Figure 1 shows CALIOP backscatter intensity profiles (Figure 1a) and scene classifications for a 1-h segment of a 27 April 2007 CALIPSO orbit. It began in darkness over North America, crossed the Pacific and Antarctica into daylight, and ended in the Indian Ocean. The scene classifications (Figure 1b), which show cloud and aerosol locations, are overlaid with black dots corresponding to Z_{top} from CERES-MODIS for optically thick, single-layer ice clouds. These are evident as the gray areas underneath the clouds. The absence of black dots indicates that the cloud is liquid water, multilayered, or optically thin cirrus. Generally, Z_{top} is 1–2 km below the CALIPSO top Z_{topCAL}.

[9] The cloud-top height pairs for all even days during April 2007 are plotted in Figure 2 as density scatter plots with linear regression fits. In Figure 2a, the average difference between the 15,367 Z_{topCAL} and their Z_{eff} pairs increases slightly with increasing altitude. The mean differ-

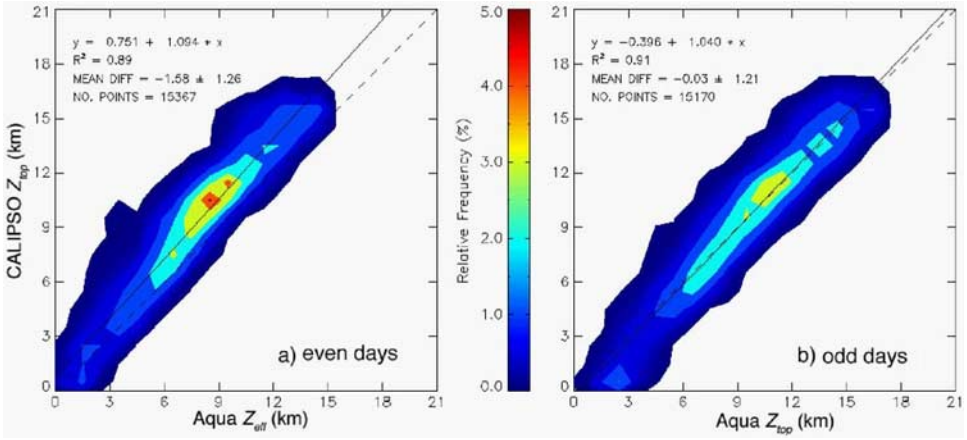

Figure 2. Scatter plots of CALIPSO optically thick non-polar cloud-top altitudes during April 2007 versus (a) Z_{eff} for even days and (b) Z_{top} computed from Z_{eff} using equation (1) for odd days.

ence, $Z_{eff} - Z_{topCAL}$, is -1.58 ± 1.26 km. The linear regression fit plotted over the data,

$$Z_{top} = 1.094 Z_{eff} + 0.751 \text{ km}, \quad (1)$$

yields a squared linear correlation coefficient $R^2 = 0.89$. According to equation (1), the difference ΔZ between Z_{top} and Z_{eff} rises from ~1.25 km for $Z_{eff} = 5$ km to more than 2 km for $Z_{eff} > 14$ km.

[10] Applying equation (1) to Z_{eff} in Figure 1b yields the new values in Figure 1c that are generally very close to the corresponding Z_{topCAL}. Figure 2b compares the 15,170 values of Z_{topCAL} and Z_{top} computed with equation (1) for all April 2007 odd-day data. For $Z_{topCAL} > 3$ km, the data are centered along the line of agreement, while lower cloud heights are overestimated. The correction yields a mean difference of -0.03 ± 1.21 km and $R^2 = 0.91$. This empirical correction effectively eliminates the bias and slightly reduces the random error in the estimated Z_{top}. The correction is robust in that it applies well to two independent datasets.

[11] For $Z_{eff} < 3$ km, the data are centered on the line of agreement in Figure 2a indicating no correction is needed. The correction results in unphysical values at those altitudes and should not be applied. This overestimation is due to uncertainties in the atmospheric profile of temperature in the lower layers [e.g., *Dong et al.*, 2008] or to misclassification of supercooled-liquid water or mixed-phase clouds as ice clouds by the CERES-MODIS *Aqua* algorithm. The basic assumption that the correction is for ice clouds would be violated for those and other low-level clouds. The tops of water clouds are unlikely to be more than a few hundred meters above Z_{eff} [e.g., *Dong et al.*, 2008]. For low clouds, a better estimate of Z_{eff} and a more accurate phase classification are needed before applying a correction to obtain Z_{top}. That effort is beyond the scope of this paper.

[12] To minimize the impact of low-altitude temperature and phase uncertainties, the regression was performed using the even-day data (13,046 samples) only for ice clouds with effective pressures, $p_{eff} < 500$ hPa, yielding

$$Z_{top} = 1.041\ Z_{eff} + 1.32 \text{ km}. \quad (2)$$

[13] Applying equation (2) to odd-day clouds having $p_{eff} < 500$ hPa yields an average difference of -0.08 ± 1.15 km, a value nearly equal to the mean difference of -0.13 ± 1.14 km that would be obtained by applying equation (1) to the same odd-day dataset. If equation (2) is used to estimate Z_{top} for *all* of the odd-day data, the mean difference is 0.07 ± 1.24 km. The results are essentially the same for both fits. The 500-hPa cutoff effectively precludes the introduction of any new low-cloud height biases.

4. Discussion

[14] The instantaneous differences can mainly be attributed to uncertainties in the temperature profiles used to convert temperature to altitude, data spatial mismatches, VZA dependencies, and variations in cloud microphysics. The small portions of the satellite pixel sampled by the narrow lidar footprint can cause some significant differences if cloud height varies within the pixel. Errors in the temperature profiles can move Z_{eff} up or down. For example, some Z_{eff} values between 6 and 14 km in Figure 2a are below their Z_{topCAL} counterparts and account for ~1 km of the range in ΔZ. It could also account for some of the extreme overestimates. This type of error will occur some of the time since the temperature profiles are based on numerical weather analysis assimilation of temporally and spatially sparse observations. The VZA has little impact here.

[15] To examine the impact of cloud microphysics on ΔZ, radiative transfer calculations were performed by applying the Discrete Ordinates Radiative Transfer (DISORT [*Stamnes et al.*, 1988] method to an example case. For a given layer, the thickness can be expressed as

$$\Delta z_i = 4\delta\ D_{ei} \Delta\ \tau_i / 6Q\ \text{IWC}_i, \quad (3)$$

where $\Delta\tau_i$ is the visible optical depth for cloud layer i, the visible extinction efficiency Q has a value of ~2 [e.g., *Minnis et al.*, 1998], IWC_i is the layer ice water content, the density of ice is $\delta = 0.9$ g cm^{-3}, and D_{ei} is the effective diameter of the ice crystals in the cloud layer.

[16] The DISORT calculations assumed an 8-km thick cloud extending to 13 km in a tropical atmosphere. The

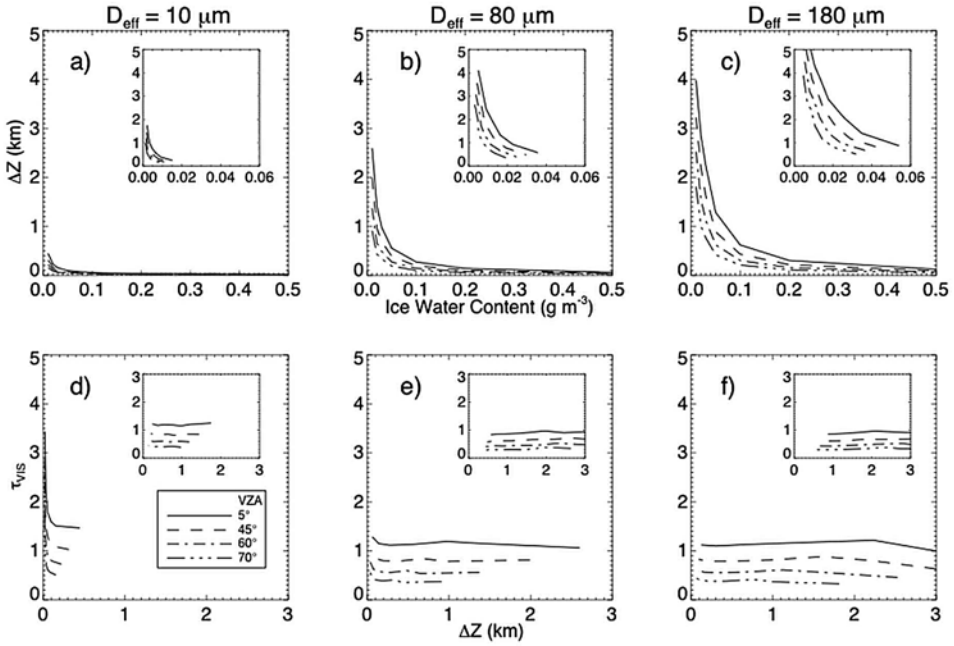

Figure 3. Theoretical variation of (a–c) cloud-top/effective height difference (ΔZ) as function of IWC and (d–f) optical depth of cloud layer above Z_{eff} as function of ΔZ. Main panels are for uniform IWC in the cloud, while insets are for IWC decreasing with increasing height in the cloud.

cloud was divided into 198 layers with Δz_i decreasing from less than 110 m at the base to 40 m at the top. The bottom-layer optical depth was specified at 12 to ensure that the cloud is optically thick. T_{eff} was determined for a range of IWC and three values of D_e using the same mean IWC but with three IWC profiles: IWC decreasing linearly from the layer above the base to cloud top, uniform IWC, and IWC increasing from the layer above the base to the top. Z_{eff} was determined from T_{eff} and the simulated cloud-top height correction is $\Delta Z = 13$ km $- Z_{eff}$. The optical depth (IWC) of the layer above Z_{eff}, the top layer, is the sum of τ_i (IWC_i) above Z_{eff}. Figure 3 shows the results for both uniform and decreasing-with-height IWC. Assuming that ~1.5 km of the range in ΔZ (Figure 2a) is due to inaccurate temperature profiles, the observed range is ~4.5 km. That extreme value of ΔZ could occur for $D_e = 180$ μm and IWC = 0.01 gm^{-3} (Figure 3c) or for smaller values of IWC and D_e (Figure 3b), but is unlikely for very small particles (Figure 3a). The average bias at $Z_{eff} = 14$ km (Figure 2a) is 2.1 km, a value that can be explained, at VZA = 14°, with uniform or decreasing IWC = 0.014 gm^{-3} and $D_e = 80$ μm (Figure 3b), or with smaller or larger values of IWC and D_e. For a given value of IWC, ΔZ in Figures 3a–3c is similar for both uniform and decreasing IWC profiles, except that, for a given ΔZ, the IWC is slightly smaller for the decreasing case. For the increasing-with-height case (not shown), ΔZ rapidly approaches zero with increasing IWC for all particle sizes.

[17] The decreasing-with-height IWC profile is probably most realistic, however, for simplicity, only the uniform IWC case results are considered in the following calculations. Although its value at 5 km is 62 μm, the CERES-MODIS observed mean D_e varies almost linearly from 55 μm at $Z_{eff} = 6$ km to 76 μm at 12.6 km, then down to 64 μm at 15 km (not shown). At 14 km, $D_e \sim 68$ μm, requiring IWC to be ~ 0.011 gm^{-3}. At $Z_{eff} = 9$ km, $\Delta Z = 1.6$ km and $D_e = 68$ μm, requiring IWC = 0.019 gm^{-3}. Since the optical depth corresponding to ΔZ is relatively constant (Figure 3d and other IWC cases), IWC can be estimated at each altitude using the proportional relationship

$$\mathrm{IWC} = kD_e/\Delta Z, \tag{4}$$

where ΔZ is determined from equation (1), D_e is the mean at Z_{eff}, and the proportionality constant k was determined from equation (4) to be 0.000334 gm^{-3}, using the estimate of IWC for $Z_{eff} = 14$ km and $D_e = 68$ μm. Values of uniform IWC were estimated for $Z_{eff} = 5$–15 km and fitted using a third order polynomial regression to obtain

$$\mathrm{IWC} = 0.018 \text{ gm}^{-3} - 0.000474\, Z_{eff}, \tag{5}$$

where Z_{eff} is in km. The R^2 equals 0.77 indicating that the average IWC is strongly dependent on cloud height. This fit does not apply below 5 km. While the mean IWC varies between 0.01 and 0.02 gm^{-3}, it is somewhat sensitive to the IWC vertical profile and much larger or smaller values of IWC could result from any individual CERES-MODIS/CALIPSO data pair.

[18] The behavior of (5) is not surprising given that IWC has been observed to decrease with decreasing cloud temperature. (T_{eff} was not used as the independent variable

here because the height differences were more highly correlated with Z_{eff} than with T_{eff}.) *Heymsfield and Platt* [1984] reported that the mean IWC in cirrus clouds varied from 0.027 gm^{-3} at T = −25°C to 0.001 gm^{-3} at −58°C and that IWC variability at a given temperature was typically an order of magnitude or greater. *Wang and Sassen* [2002] found IWC ranging from 0.017 to 0.001 gm^{-3} between −20 and −70°C for comparable clouds. *Garrett et al.* [2005] observed IWCs up to 0.3 gm^{-3} in a thick anvil cloud, while smaller values, ranging from 0.0001 to 0.02 gm^{-3}, were observed by *McFarquhar and Heymsfield* [1996] in the top 2 km of three tropical anvils. The mean IWC values estimated here for the top portions of thick ice clouds are well within the range of observations. The variation in the observed IWCs can also explain much of the random error seen in Figure 2b.

[19] Figures 3e and 3f show that the top-layer τ, constant at ∼1.15 for D_e = 80 and 180 μm, increases to 1.5 for D_e = 10 μm (Figure 3d) and to larger values when IWC < 0.01 gm^{-3}. The corresponding values for the decreasing IWC case are 0.9 and 1.2 for D_e = 80 and 10 μm, respectively, and slightly greater for the increasing IWC case. The values of τ for the larger particles are close to that used by *Sherwood et al.* [2004] to estimate where Z_{eff} should be relative to the lidar-observed top for convective anvils. The difference is mostly due to scattering. Based on the lidar-derived optical depths, *Sherwood et al.* [2004] concluded that the large values of ΔZ, similar to those in Figure 2a, did not correspond to $\tau = 1$, but to $\tau \geq 10$. Given the above analysis and the observed range of IWC, it appears that an average value of 2 km for ΔZ is quite reasonable and corresponds to $\tau \sim 1$ for the size of ice crystals retrieved with VISST. For the matched CALIPSO-CERES data used here, the mean height where the CALIPSO beam was fully attenuated is 1.3 km below Z_{eff}, a value much greater than the 150 m calculated for the airborne lidar used in the *Sherwood et al.* [2004] analysis. It is not clear why that earlier study produced such different results from the current analysis, but may be due to assumptions used in the τ retrievals from the airborne lidar or differences in power between it and the CALIOP. Nevertheless, the current results are consistent with the expected values of IWC near cloud top.

[20] While the small range (9°–19°) in VZA for this study precludes development of an empirical correction for VZA dependence, the plots in Figure 3 suggest a simple cosine variation of ΔZ with VZA. Thus, calculating Z_{top}' using either equations (1) or (2), the VZA-corrected estimate of Z_{top} is

$$Z_{top} = Z_{eff} + \Delta Z, \tag{6}$$

where $\Delta Z = (Z_{top}' - Z_{eff})\cos(\mathrm{VZA})$. Validating equation (6) will require a comprehensive combined imager-lidar dataset having a wide range of VZAs.

5. Concluding Remarks

[21] The effective cloud radiating height, Z_{eff}, may be adequate for radiative transfer calculations in climate or weather models, but the physical boundaries of a cloud are needed to determine where condensates form and persist. The upper boundary is inadequately represented by Z_{eff} for ice clouds. A simple parameterization was developed that uses Z_{eff} to provide, on average, an unbiased estimate of Z_{top} for optically thick ice clouds. It complements other parameterizations used to estimate Z_{top} for optically thin cirrus. The random errors in Z_{top} determined with the new parameterization are consistent with the variations in IWC observed near cloud top in previous in situ measurements. Reducing the instantaneous uncertainty in Z_{top} may be possible using combinations of different spectral channels or dual-angle views, but the reduction will be limited by the accuracy of the temperature profile. When applied, the parameterization estimate of Z_{top} should have some level above the tropopause as an upper limit to minimize unrealistic results. If the observed cloud penetrates into the stratosphere, however, Z_{eff} and, hence, Z_{top} can be underestimated because the VISST selects Z_{eff} as lowest the altitude where T_{eff} is found in the sounding. Additionally, the correction should not be applied to low-level clouds. Although this correction for Z_{top} is a function of Z_{eff} determined from the 11-μm brightness temperature, it is probably applicable to Z_{eff} determined using other techniques such as CO_2 slicing. Although only 1 month of CALIPSO data was used here, the results appear robust. Testing with data from other seasons is required to confirm that contention and data from other satellites, that are not near the CALIPSO ground track, would be needed to verify the formulation for off-nadir angles. With an expanded dataset, it may also be possible to refine the correction in terms of cloud type (e.g., cirrus, anvil, or convective core).

[22] **Acknowledgments.** This research was supported by NASA through the NASA Energy and Water Cycle Studies Program and the CALIPSO and CERES projects.

References

Dong, X., P. Minnis, B. Xi, S. Sun-Mack, and Y. Chen (2008), Comparison of CERES-MODIS stratus cloud properties with ground-based measurements at the DOE ARM Southern Great Plains site, *J. Geophys. Res.*, *113*, D03204, doi:10.1029/2007JD008438.

Garrett, T. J., et al. (2005), In situ measurements of the microphysical and radiative evolution of a Florida cirrus anvil, *J. Atmos. Sci.*, *62*, 2352–2372.

Heymsfield, A., and C. M. R. Platt (1984), A parameterization of the particle size spectrum of ice clouds in terms of the ambient temperature and the ice water content, *J. Atmos. Sci.*, *41*, 846–855.

McFarquhar, G. M., and A. J. Heymsfield (1996), Microphysical characteristics of three anvils sampled during the central equatorial Pacific experiment, *J. Atmos. Sci.*, *53*, 2401–2423.

Minnis, P., P. W. Heck, and E. F. Harrison (1990), The 27–28 October 1986 FIRE IFO cirrus case study: Cloud parameter fields derived from satellite data, *Mon. Weather Rev.*, *118*, 2426–2447.

Minnis, P., et al. (1995), Clouds and the Earth's Radiant Energy System (CERES) algorithm theoretical basis document, volume III: Cloud analyses and radiance inversions (subsystem 4), in *Cloud Optical Property Retrieval (Subsystem 4.3)*, *NASA Ref. Publ.*, *RP 1376*, vol. 3, 135–176.

Minnis, P., D. P. Garber, D. F. Young, R. F. Arduini, and Y. Takano (1998), Parameterizations of reflectance and effective emittance for satellite remote sensing of cloud properties, *J. Atmos. Sci.*, *55*, 3313–3339.

Minnis, P., et al. (2006), Overview of CERES cloud properties from VIRS and MODIS, paper presented at 12th Conference on Atmospheric Radiation, Am. Meteorol. Soc., Madison, Wis., 10 –14 July.

Rossow, W. B., and R. A. Schiffer (1999), Advances in understanding clouds from ISCCP, *Bull. Am. Meteorol. Soc.*, *80*, 2261–2287.

Sherwood, S. C., J.-H. Chae, P. Minnis, and M. McGill (2004), Underestimation of deep convective cloud tops by thermal imagery, *Geophys. Res. Lett.*, *31*, L11102, doi:10.1029/2004GL019699.

Stamnes, K., S. C. Tsay, W. Wiscombe, and K. Jayaweera (1988), Numerically stable algorithm for discrete-ordinate-method radiative transfer in multiple scattering and emitting layered media, *Appl. Opt.*, *27*, 2502–2509.

Sun-Mack, S., et al. (2007), Integrated cloud-aerosol-radiation product using CERES, MODIS, CALISPO, and CloudSat data, *Proc. SPIE Int. Soc. Opt. Eng.*, *6745*, 1–11.

Vaughan, M., et al. (2004), Fully automated analysis of space-based lidar data: An overview of the CALIPSO retrieval algorithms and data products, *Proc. SPIE Int. Soc. Opt. Eng.*, *5575*, 16–30.

Wang, Z., and K. Sassen (2002), Cirrus cloud microphysical property retrieval using lidar and radar measurements. part II: Midlatitude cirrus microphysical and radiative properties, *J. Atmos. Sci.*, *59*, 2291–2302.

Winker, D. M., W. H. Hunt, and M. J. McGill (2007), Initial performance assessment of CALIOP, *Geophys. Res. Lett.*, *34*, L19803, doi:10.1029/2007GL030135.

Y. Chen, S. Sun-Mack, and C. R. Yost, Science Systems and Applications, Inc., Hampton, VA 23666, USA.

P. Minnis, NASA Langley Research Center, Hampton, VA 12681-0001, USA. (patrick.minnis@nasa.gov)